Int. J. Heat Mass Transfer. Vol. 33, No. 9, pp. 2001–2018, 1990
Printed in Great Britain

0017-9310/90 $3.00 + 0.00

Rate correlation for condensation of pure vapor on turbulent, subcooled liquid

J. STEVEN BROWN, BOO CHEONG KHOO† and AIN A. SONIN‡
Department of Mechanical Engineering, Massachusetts Institute of Technology, Cambridge, MA 02139, U.S.A.

(*Received* 6 *March* 1989 *and in final form* 6 *November* 1989)

Abstract—An empirical correlation is presented for the condensation of pure vapor on a subcooled, turbulent liquid with a shear-free interface. The correlation expresses the dependence of the condensation rate on fluid properties, on the liquid-side turbulence (which is imposed from below), and on the effects of buoyancy in the interfacial thermal layer. The correlation is derived from experiments with steam and water, but under conditions which simulate typical cryogenic fluids.

1. INTRODUCTION

CONDENSATION of pure vapor at a turbulent liquid interface is a liquid-side heat transfer process, the rate being limited by the turbulent transport of the latent heat from the interface to the bulk of the liquid. Theoretically, this is still an unsolved problem, largely because the structure of the turbulence very near the free surface is still open to speculation. At lower turbulence intensities the condensation problem is further complicated by stable thermal stratification at the interface, with attendant turbulence damping. Simplistic models have been proposed for the analogous gas absorption problem, where thermal stratification is absent [1–8]. However, each of these models is tailored largely to specific experimental conditions. The models disagree with each other, and there is no consensus on a unified model which expresses the condensation rate in terms of the local turbulence parameters and fluid properties (e.g. see ref. [9]). Progress toward such a model has been hindered not only by the lack of understanding of the interfacial turbulence structure, but also by the fact that accurate comparison with experiment has been difficult: the turbulence parameters which appear in a general model (e.g. turbulence intensity and turbulence macroscale) have not been directly measured in most investigations of condensation.

Simultaneous data on vapor condensation rate and liquid-side turbulence are relatively scarce. Thomas [10] made measurements with steam and water in several different systems in which turbulence was imposed on the liquid from below, without shear on the interface. Jensen and Yuen [11] report measurements in a channel flow in which the liquid-side turbulence was induced largely by interfacial shear from the steam side. Ueda *et al.* [12], Mizushina *et al.* [13], Komori *et al.* [14, 15] and Ogino [16] have published significant basic data on the turbulence structure in a channel flow with interfacial heat transfer. They did not, however, report simultaneous measurements of the heat transfer rate at the interface, and their measurements of turbulent diffusivity do not cover the very thin region near the free surface where most of the temperature drop occurs when buoyancy effects are not dominant.

More recently, Sonin *et al.* [9] investigated the condensation of pure steam on a shear-free water interface, on which a calibrated turbulence was imposed from below. Using relatively high turbulence intensities where buoyancy effects were negligible, they concluded that the condensation rate could be correlated in terms of a constant Stanton number based on the liquid-side turbulence intensity.

In this paper we present a more general empirical correlation for the rate of pure vapor condensation on a turbulent subcooled liquid. The correlation accounts not only for the dependence on the interfacial turbulence conditions, but also establishes the dependence on liquid-side Prandtl number and buoyancy. One of the major objectives of this work has been to obtain a rate correlation that can be applied to predict the condensation rate of cryogenic fluids under a broad range of turbulence conditions.

The present work is based on experiments with steam and water, and generalized to other fluids by means of scaling laws (Section 5). Our apparatus is similar to the one used in ref. [9], but experimental accuracy has been improved, the system has been modified to operate over a range of saturation conditions, and our data correlation is based on more precise information on the turbulence structure in the system (Section 3). Our correlation covers the scaling

† Presently at the Department of Mechanical and Production Engineering, National University of Singapore.
‡ Author to whom correspondence should be addressed.

NOMENCLATURE

c_p	specific heat at constant pressure [J kg^{-1} K^{-1}]
d	nozzle exit diameter, Fig. 1 [m]
D	test cell inside diameter, Fig. 1 [m]
f	frequency [Hz]
g	gravitational (or reference frame) acceleration [m s^{-2}]
Gr	Grashof number, equation (39)
h_{fg}	latent heat of condensation [J kg^{-1}]
Ja	Jakob number, equation (17)
k	turbulence intensity in k–ε model [m^2 s^{-2}]
l	turbulence macroscale [m]
L	length scale in k–ε turbulence model, $k^{3/2}/\varepsilon$ [m]
$\dot{m}$	condensation mass flux across interface [kg s^{-1} m^{-2}]
Q	volume flow rate circulating through system, Fig. 1 [m^3 s^{-1}]
r	radial coordinate [m]
$R(t)$	Eulerian autocorrelation function measured at a fixed point, equation (8)
Re	Reynolds number, equation (17)
Re_*	system Reynolds number, $Q\,dv$
Ri	Richardson number, equation (17)
St	condensation Stanton number, equation (17)
St_0	reduced Stanton number, equation (37)
t	time [s]
$\tilde{t}$	characteristic time, equations (7) and (9) [s]
T	absolute temperature [K]
T_b	value of T_B extrapolated to the interface, Fig. 7(b) [K]
T_B	temperature in bulk of liquid, outside interfacial layer, Fig. 7(b) [K]
T_s	liquid saturation temperature [K]
ΔT	liquid subcooling, $T_s - T_b$ [K]
u_c	condensation induced bulk flow, $\dot{m}/\rho_b$, equation (20) [m s^{-1}]
v	r.m.s. value of either the horizontal or vertical component of turbulent velocity [m s^{-1}]
v_b	value of v extrapolated from the bulk liquid to the surface disregarding the interfacial layer, Fig. 7(a) [m s^{-1}]
y	coordinate measured vertically downward from the surface into the bulk liquid, Fig. 1 [m]
z	coordinate measured vertically upward from the nozzle exit into the bulk liquid, Fig. 1 [m]
z_s	elevation of surface from nozzle exit, Fig. 1 [m].

Greek symbols

α	thermal diffusivity [m^2 s^{-1}]
α_T	turbulent thermal diffusivity, equation (22) [m^2 s^{-1}]
α_{TB}	turbulent thermal diffusivity outside the interfacial layer, Fig. 7(c) [m^2 s^{-1}]
β	coefficient of thermal expansion [K^{-1}]
δ	thermal layer thickness, equation (18) [m]
δ_v	viscous layer thickness [m]
ε	viscous dissipation rate in k–ε model [m^2 s^{-3}]
λ	thermal conductivity [kg m s^{-3} K^{-1}]
Λ	integral turbulence length scale, equation (9) [m]
μ	viscosity [kg m^{-1} s^{-1}]
ν	kinematic viscosity [m^2 s^{-1}]
ρ	density [kg m^{-3}]
τ	statistical property, equations (31) and (32) [s]
$\phi(Re_*)$	function defined in equation (3)
$\Phi(f)$	Eulerian time spectrum, equation (11) [m^2 s^{-1}].

Subscripts

b	liquid at bulk temperature (extrapolated to interface)
g	vapor
s	liquid at saturation temperature.

parameters characteristic of most cryogenic fluids, and establishes the dependence of the condensation rate on the liquid and vapor properties, the liquid-side turbulence intensity and turbulence macroscale, and the effects of buoyancy.

2. TEST CELL

Experiments were performed with steam and water in a test cell (Fig. 1) which is geometrically similar to those used in ref. [9]. The cell consists of a pyrex tube of inside diameter D, partially filled with water. A statistically steady turbulence is generated in the water by a single submerged nozzle located far below the interface ($z_s \gg d$, where z_s is the interface elevation relative to the nozzle exit and d the nozzle diameter), so that the region near the interface is in the far field of the jet. The water is circulated in a closed loop, with the temperature controlled by a heat exchanger. Sufficiently far from the nozzle (about $z > 3D$), this system produces an essentially bulk-flow-free turbulence which is approximately isotropic in the hori-

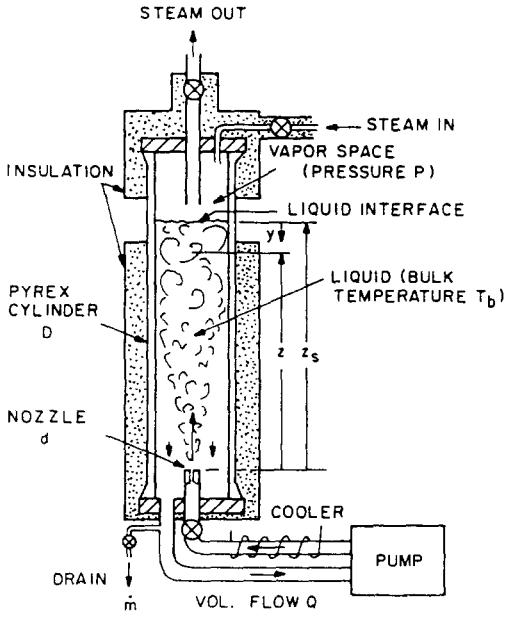

FIG. 1. Schematic of test cell.

zontal plane but decays with elevation z from the nozzle. The turbulence intensity can be easily controlled via the volume flow rate through the nozzle. The integral length scale is locked to the tube diameter (see Section 3) and can be controlled via system size. All the condensation measurements reported here were made with the water elevation at 3.67 system diameters above the nozzle exit, i.e. with $z_s/D = 3.67$.

Two test cells were used for the condensation tests, with diameters D of 10.2 and 3.8 cm and nozzle exit diameters d of 0.42 and 0.16 cm, respectively, so that the ratio D/d was 24 as in the systems of ref. [9]. A larger cell with $D = 15.3$ cm was used for the turbulence study with a laser Doppler velocimeter. The smaller systems were required for the condensation tests to attain the higher pressures and temperatures at which water has the low Prandtl numbers of liquid cryogens. All three test cells were geometrically similar, including the nozzle diameter ($D/d = 24$) and nozzle geometry (length/$d = 6.3$, with the inlet lip rounded with a radius of curvature of about $0.5d$).

Pure steam from the MIT steam supply was admitted to the test section, and allowed to exhaust via a central port at a slow rate (see also Section 4). The steam was passed through a commercial steam–water separator and into a 75 dm^3 settling tank before being routed to the test cell. The settling tank was vented slowly at the bottom to help remove residual moisture, etc. All parts of the steam supply system, from upstream of the settling tank to the top part of the test cell, were heated with strip heaters and insulated. The water was tap water. Operating pressures ranged from 0.11 to 0.37 MPa, corresponding to saturation temperatures from 103 to 141°C, and bulk water temperatures ranged from 37 to 118°C.

3. TURBULENCE CALIBRATION

3.1. *Video measurements of r.m.s. velocity at centerline*

Consider the turbulent flow field in the liquid at an elevation z which is sufficiently far from the nozzle to be in the far field of the jet (i.e. $z \gg d$), but not so close to the surface that z is in the interfacial layer. Sonin *et al.* [9] argued that, at the high Reynolds numbers where the jet is fully turbulent, the r.m.s. value v of a component of the velocity fluctuation will obey the scaling law

$$v(r, z) = (Q/Dd) f(Re_*, r/D, z/D) \tag{1}$$

where Q is the volume flow rate circulating through the system (Fig. 1), and

$$Re_* = Q/\nu \tag{2}$$

is a system Reynolds number based on the characteristic speed Q/Dd. Experiments showed that at $3.1 < z/D < 4.2$, the r.m.s. velocity near the system centerline is given by

$$v(0, z) \simeq \phi(Re_*)(Q/Dd)\, e^{-1.2z/D}. \tag{3}$$

Sonin *et al.* [9] seeded the flow with 3 mm diameter polypropylene spheres (specific gravity 0.91), filmed the motion at 120 frames per second, and deduced the vertical and horizontal velocity components of the particles by measuring particle displacement between successive frames. Their measurements in a 15.3 cm diameter cell showed that $\phi(Re_*) \simeq 21.8$ for $Re_* > 2.5 \times 10^4$. Data taken in a 3.8 cm diameter cell at lower Reynolds numbers indicated higher values of $\phi(Re_*)$, of the order of 30–35, suggesting that $\phi(Re_*)$ increases at lower Reynolds numbers. The nozzle in their smaller cell was, however, not exactly similar in length and inlet shape to the one in the larger, and the seed particles were fairly sizable (8% of D) relative to the smaller cell's diameter.

We have repeated the video measurements in a 3.8 cm cell which is completely similar to the larger one, using smaller polystyrene spheres (average diameter 0.4 mm, actual diameter 0.1–0.8 mm) with specific gravity 1.05. The video camera was focused on the test cell axis and data were taken near the centerline, in a 'window' with horizontal boundaries at $z/D = 3.67 \pm 0.13$ and vertical boundaries at $r/D = \pm 0.13$. The free surface was set at a height $z_s/D = 5.8$, i.e. well above the test window, so that the velocity measurements would represent data in the bulk of the liquid far below the interface.

Figure 2 shows the data for the r.m.s. values of the fluctuating vertical and horizontal velocity components, expressed in the dimensionless form $\phi(Re_*)$ defined by equation (3). The new data for the smaller system are in the region $Re_* < 2.5 \times 10^4$; the data for $Re_* > 2.5 \times 10^4$ are those taken by Sonin *et al.* [9] in their larger system. Each point in our new data set is derived from a minimum of 200 velocity measurements, vs 60 in the data of Sonin *et al.* [9].

The new data do not show a clear rise in $\phi(Re_*)$ at

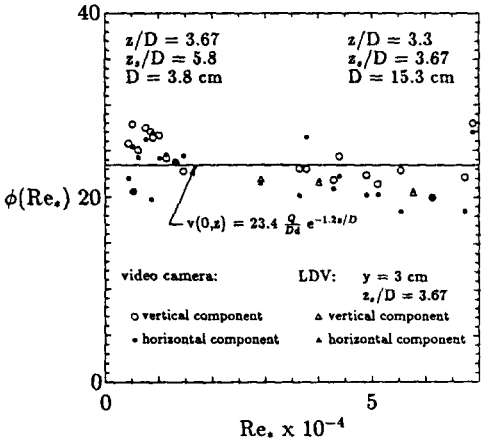

FIG. 2. Calibration of turbulence intensity at centerline of test cell.

lower system Reynolds numbers. The average value based on all data points in both data sets is

$$\phi(Re_*) \simeq 23.4 \quad (4\times 10^3 < Re_* < 7\times 10^4). \quad (4)$$

The standard deviation of the data is 2.70, or 12% of the mean, which is reasonably consistent with the inverse square root of the number of measurements on which each data point is based. Taken separately, the lower Reynolds number data set does show a somewhat higher average value of $\phi(Re_*)$ than the higher Reynolds number set, 24.5 vs 21.8. This might suggest a slight decline in $\phi(Re_*)$ with increasing Re_*. However, the difference is within the standard deviation of the data taken as a whole, and we adopt equation (4) in what follows.

The r.m.s. values of the vertical and horizontal fluctuating velocities differ by less than one standard deviation of the data scatter. The mean velocity components were found to be smaller than the standard deviation of the r.m.s. values. In the new data set, the average mean horizontal velocity was 0.7 cm s^{-1}, while its standard deviation was 0.9 cm s^{-1}. This is to be compared with an average r.m.s. fluctuating velocity component of 9 cm s^{-1}. The average value of the mean vertical velocity measurements was 0.5 cm s^{-1} (downward), with a standard deviation of 0.5 cm s^{-1}. The data are thus consistent with the view that at the higher elevations ($z/D > 3$, say), turbulent fluctuations dominate over any remaining mean circulatory flow, and the turbulence is approximately isotropic.

3.2. *LDV measurements*

Laser Doppler velocimetry was used in a cell which was essentially identical to the larger one of the two used in ref. [9] ($D = 15.3$ cm) except that a flat plexiglass window was mounted on its side between the elevations $z = 39.5$ and 72.5 cm, at a (minimum) distance of 7.2 cm from the axis. Since the test cell's nominal radius was 7.6 cm, the window did not cause a significant perturbation in the cylindrical geometry.

The LDA was a back-scattered two-color system consisting of a Lexel model 95 ion laser and DISA-made optics, with the counter linked to a portable DEC MINC-11 mini-computer. The use of two beam expanders in series resulted in a very small measuring volume, $40\times 40\times 600$ μm. Traverses through the cell were made by moving the test cell, which was mounted on a test table with vernier movements in three orthogonal directions as well as rotation in a horizontal plane. The effect of pump vibration on the test cell and the optics was minimized by resting the pump on vibration absorbers and connecting it to the test cell via an 8 ft. long stainless steel flexible hose. Preliminary tests of the LDA system were carried out with the test cell replaced by a plexiglass disc which was filled with water and rotated at a known angular velocity. LDA readings of velocity were recorded with the pump turned off, and were found to agree with the imposed velocity to within 3%. The r.m.s. value of the velocity fluctuations (in this case caused by system noise) was about 5% of the mean. This figure did not change significantly when the centrifugal pump was turned on, which suggested that pump vibration was not a problem.

For seedlings we used aluminum particles of size 3 μm, which gave a signal-to-noise ratio of about 5; 1 μm particles were also tested, but were found to give a poorer signal-to-noise ratio.

3.2.1. *Centerline turbulence intensity.* Figure 3 shows data for the distribution of r.m.s. fluctuating velocity as a function of depth below the interface, taken along the system's axis. The surface was at an elevation $z_s/D = 3.67$. Each data point is the average of five measurements of r.m.s. velocity, with each measurement derived from 10^4 velocity samples. The bars show the maximum and minimum values of the five measurements. Also shown on the figures as a broken line is the correlation equation (3) with $\phi(Re_*)$ taken as 21.8, the average value of the data taken in this system.

At sufficient depths the turbulence distribution is approximately isotropic and decays gradually with increasing elevation z (decreasing y), in agreement with equation (3). Closer to the surface one enters the interfacial layer, in which the vertical velocity fluctuations are damped (the surface maintained an approximately horizontal state in all these tests) and their kinetic energy is imparted to the velocity components parallel to the surface, which are not constrained at the interface (see also ref. [14]). Figure 3 suggests that the interfacial layer has a depth of about $0.1D$ in our type of system. The mean velocity components are not shown, but are bounded by -0.01 and 0.01 m s^{-1}, that is, they are small compared with the r.m.s. velocity fluctuations.

Figure 2 shows six LDV data points for $\phi(Re_*)$. These data points are derived by fitting equation (3) to each of the six data sets in Fig. 3, using only those

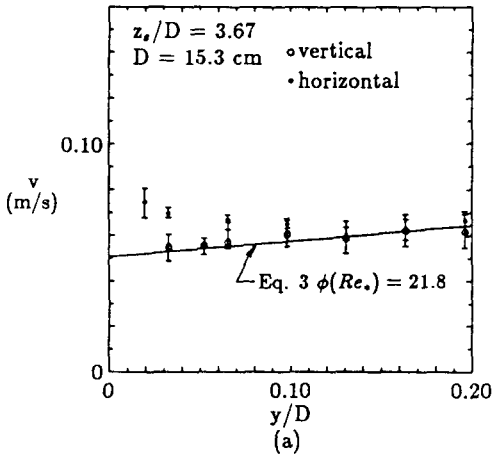

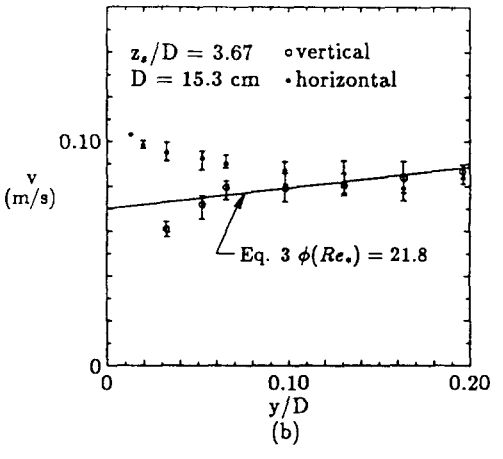

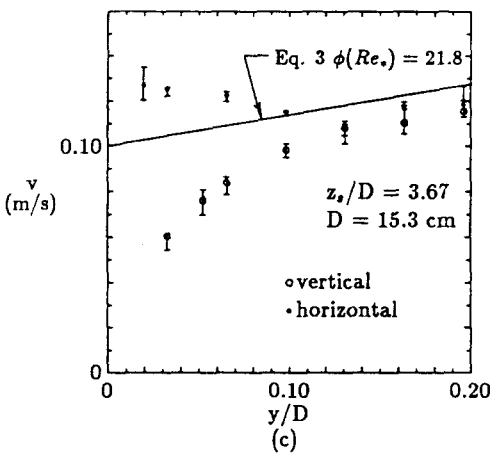

FIG. 3. Centerline distribution of r.m.s. fluctuating velocity as a function of depth below the interface for (a) $Re_* = 2.91 \times 10^4$, (b) $Re_* = 4.01 \times 10^4$, (c) $Re_* = 5.77 \times 10^4$.

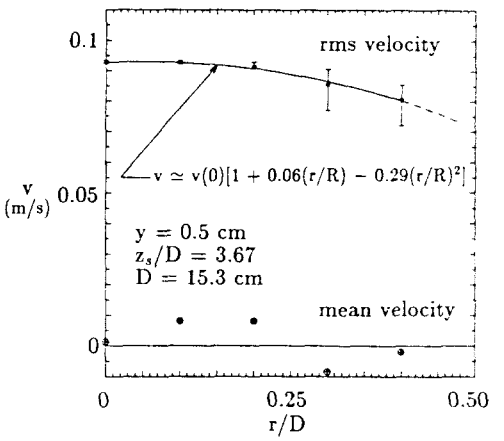

FIG. 4. R.m.s. and mean azimuthal velocities as functions of r at a depth of 0.5 cm below the interface for $Re_* = 4.01 \times 10^4$.

points which are below the interfacial layer. The results are in reasonably good agreement with $\phi(Re_*) = 21.8$, the average value of the video data taken in this system, although they fall somewhat below the line $\phi(Re_*) = 23.4$ which represents the average for all the video data.

3.2.2. *Radial distribution of turbulence intensity.* Figure 4 shows the radial distributions of both the azimuthal r.m.s. velocity and the mean azimuthal velocity at a depth of 0.5 cm. As expected, the r.m.s. velocity tends to decrease as one approaches the wall. The data in Fig. 4 can be fitted approximately with

$$v \simeq v(0)[1 + 0.06(r/R) - 0.29(r/R)^2] \tag{5}$$

where $R \equiv D/2$. This equation may be viewed as an 'outer' turbulence distribution, analogous to Coles' 'law of the wake' in shear flows [17] and must break down sufficiently close to the wall, where viscous effects must set in. By analogy with shear flows, the viscous layer thickness δ_v near the wall can be estimated from $v(0)\delta_v/\nu \sim 10$, say, where ν is the kinematic viscosity. This yields $\delta_v/R \sim O(10^{-3})$, which suggests that equation (5) may be extended fairly close to the wall before a significant departure occurs. Hence, the *average* r.m.s. velocity over the interface can be estimated as

$$v_{av} = (1/\pi R^2) \int_0^R v 2\pi r \, dr \simeq 0.90 v(0) \tag{6}$$

where $v(0)$ is the centerline value.

3.2.3. *Turbulence macroscale.* Since our measurements were restricted to a single point at a given time, we define an integral time scale as

$$\bar{t} \equiv \int_0^\infty R(t) \, dt \tag{7}$$

where

$$R(t) \equiv \langle v'(t' + t)v'(t') \rangle / v'^2 \tag{8}$$

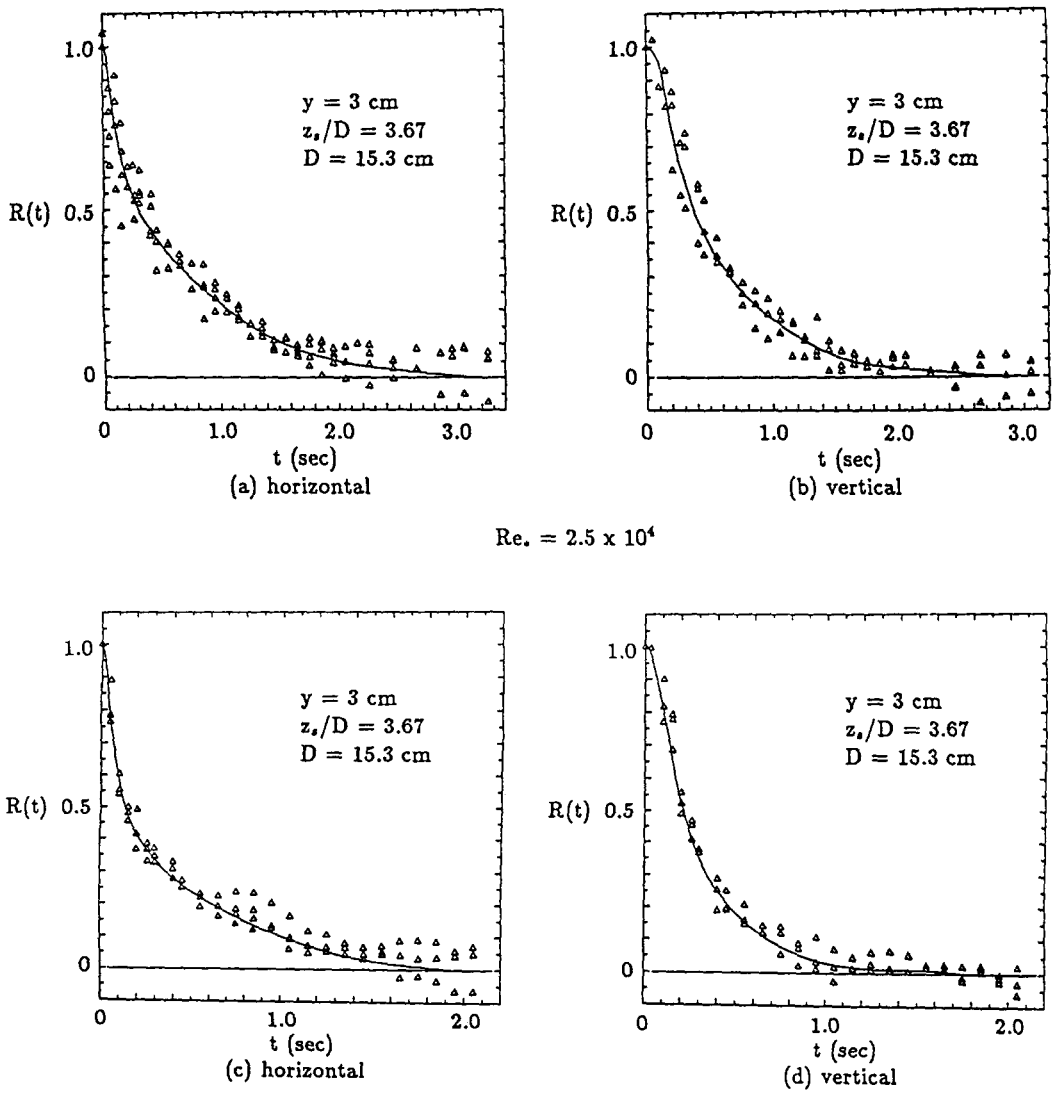

FIG. 5. Eulerian time correlation of the velocity at the centerline at a depth of 3 cm below the interface.

is the Eulerian time correlation of the velocity at a given point. Here v' represents the fluctuating velocity component in a particular direction (we shall see that the time scale is approximately independent of the choice of direction), $\langle\ \rangle$ represents ensemble averaging, and v is the r.m.s. value of v'. An integral length can now be defined as

$$\Lambda \equiv (v\tilde{t})_{t=0}. \tag{9}$$

Figure 5 shows some examples of the function $R(t)$ measured at the system centerline at a depth of 3 cm, with the interface at $z_s/D = 3.67$. Each correlation was derived from four samples of 10^4 data points each, collected at about 100 Hz. The Doppler frequency counter was adjusted to the 'combined mode', so that each Doppler burst yielded only one datum after validation. Table 1 summarizes all the results for $R(t)$, $\tilde{t}$ and Λ. These data imply that, in the neighborhood of $z/D \sim 3.6$, the integral length scale near the system centerline is approximately independent of Reynolds number, isotropic in direction (at least below the interfacial layer) and given by

$$\Lambda \simeq 0.24D. \tag{10}$$

We shall use equation (10) as the characteristic macroscale at elevations in the neighborhood of $z/D \sim 3.6$. We note that the jet spreads to fill the entire cross section of the cell at $z/D \sim 3$, and that the macroscale should become 'locked' to the system diameter at higher elevations. Equation (10) should therefore not depend on z.

3.2.4. *Turbulence spectra.* Figure 6 shows some examples of Eulerian time spectra [18]

Table 1. LDV measurements of integral time scale ($\bar{t}$) and integral length scale ($\Lambda = v\bar{t}$) in 15.3 cm diameter test cell at a depth of 3 cm below the interface. v and $\bar{t}$ are based on centerline values

v (m s^{-1})	$\bar{t} \equiv \int_0^\infty R(t)\,\mathrm{d}t$ (s)	$\Lambda = v\bar{t}$ (m)
Horizontal components:		
0.062	0.58	0.0360
0.082	0.44	0.0363
0.116	0.34	0.0393
0.160	0.24	0.0283
Vertical components:		
0.062	0.58	0.0360
0.088	0.42	0.0370
0.131	0.31	0.0405
0.191	0.20	0.0382
Average: $\Lambda = 0.0365$ m $\simeq 0.24D$		

$$\Phi(f) = \int_{-\infty}^{\infty} \exp(-\mathrm{i}2\pi f t)\langle v'(t'+t)v'(t')\rangle\,\mathrm{d}t \quad (11)$$

based on the correlation of either the vertical or horizontal component of the fluctuating velocity. Here, f is the frequency in hertz.

At a given Reynolds number, the spectra of the vertical and horizontal velocity components are approximately identical, consistent with an isotropic turbulence, and decay at high f approximately as $f^{-5/3}$, as expected in the inertial subrange [18]. The points at which the spectra 'break' from the inertial subrange at low frequencies are approximately consistent with the integral time scales of Table 1.

3.2.5. *Conclusions.* The turbulence intensity at the centerline of the system of Fig. 1 is given by equation (3), with $\phi(Re_*)$ given in Fig. 2. A constant value of $\phi(Re_*) \simeq 23.4$ provides an adequate fit of the data for $4 \times 10^3 < Re_* < 70 \times 10^3$. Equation (3) describes the r.m.s. value v of a single component of the fluctuating velocity at a point below the interfacial layer, where the turbulence is approximately isotropic, and can be used to define an extrapolated value v_b (see Section 5) of v from the bulk region to the interface.

The average value of v over the cross section is 0.90 times the centerline value.

In the central region of the test cell, the integral length scale Λ based on the product of v and the Eulerian integral time scale is $0.24D$, where D is the system diameter.

4. CONDENSATION RATE MEASUREMENT

The test cell was operated in steady state, with constant water level, by continuously draining water at a slow rate. To begin with, the condensation rate was measured by two independent methods, a 'thermal' method and a 'mass' method. The thermal method [9] is based on measuring the circulating volume flow rate and the temperature rise between the outlet and the inlet, and determining the condensation heat transfer rate from the First Law, assuming negligible heat losses from the sides and bottom of the test section (a good assumption in our tests). The mass method is based on measuring the drainage mass flow rate under steady state conditions, and assuming that it is due entirely to condensation at the interface.

These two methods generally agreed well at the high subcoolings typical of most of the data of ref. [9], but were found to depart from each other as the subcooling was decreased (bulk temperature increased), with the discrepancy being somewhat erratic. Part of this discrepancy was traced to the thermistors which were used to measure the temperature difference. A 'matched' pair were used as in Sonin *et al.* [9], but tests showed that the pair tended to become increasingly mismatched as the absolute temperature rose, and errors as large as 30% could result in the measurements of the lowest temperature differentials, which occurred at the highest bulk temperatures. For this reason, all the condensation rates reported here were measured using the mass method.

The major source of error in the mass method is water carried into the test section either by 'wet' steam, or as a result of condensation upstream of the main condensation interface. (The thermal method is not prone to such error, at least if the water inflow is not too large, because it is based on a heat rather than a mass balance and the sensible heat of any incoming water is typically very small compared with the latent heat of condensation.) These errors were eliminated by lining the walls of the steam settling tank, the steam inflow lines, and the test section walls above the water level with strip heaters and insulation, and running all tests with these surfaces superheated, so that no condensation would occur and all droplets would be vaporized before passing into the test section. Tests showed that with no wall heating (zero steam superheat), the mass method tended to overestimate the true condensation rate somewhat, but that the true value would be obtained provided the superheat was maintained at a level higher than a few °C. Note that a modest steam superheat (a few tens of degrees, say) does not affect the condensation rate at the liquid surface because the added enthalpy which is associated with the superheat is small compared with the latent heat of condensation. As a final test for the absence of condensation upstream of the bulk water surface, the pump was turned off and a steady state was attained with no turbulence on the liquid side, but with the steam exhausting slowly from the vent in the test cell (see below). No measurable condensation was detected.

Air or other noncondensables in the steam are also potential sources of error in all condensation measurements. These were eliminated in two ways. First, data were taken only after the system, including the settling tank, had been thoroughly flushed with at least 50 system volumes of steam, and the readings were

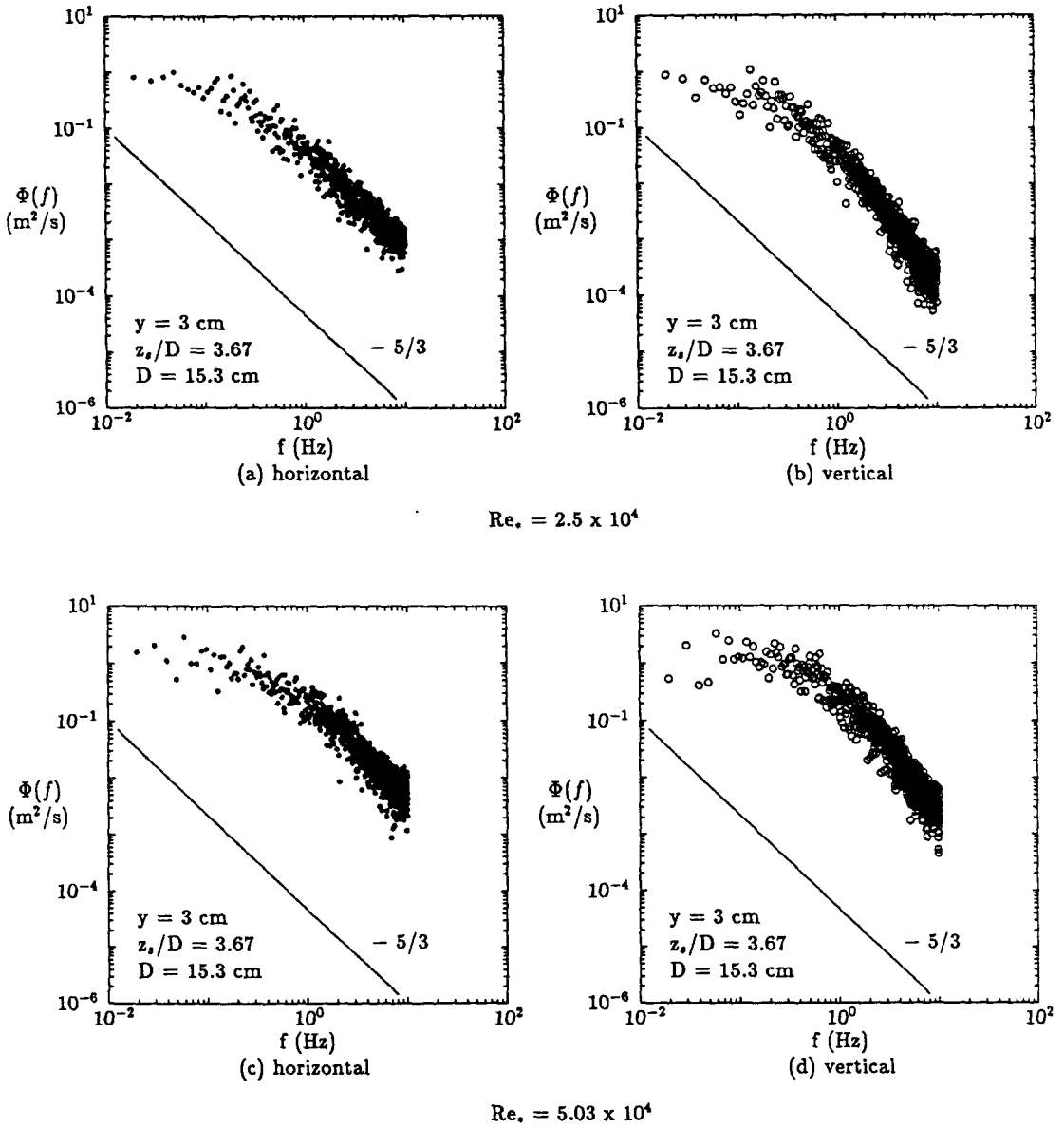

FIG. 6. Eulerian time spectrum of the velocity at the centerline at a depth of 3 cm below the interface.

invariant with time. Secondly, to prevent the gradual buildup of noncondensables which might result from even very small mass fractions of air in the steam, a small amount of steam was continuously exhausted from the test cell via a central tube fairly close to the water surface, as in ref. [9]. The exhaust rate was set empirically in a range where its magnitude had no effect on the condensation rate (the concern here being that excess steam flow rate might increase the liquid-side turbulence by shear at the surface, while too low a steam flow rate might allow noncondensables to accumulate). The second measure proved to be unnecessary, since tests with the steam exhaust closed for up to an hour showed no decrease in the condensation rate. Nevertheless, all data reported here were taken while a small amount of steam was exhausted from the cell.

Data reproducibility was checked by recording the condensation rate at a standard condition at the beginning and end of each day of runs. The r.m.s. value of the scatter in this data set was 3% of the mean.

5. CONDENSATION SCALING LAWS

We consider a pure vapor, with temperature T_g and saturation temperature T_s, in contact with its subcooled autogenous liquid. The vapor is quiescent, but drifts toward the liquid surface, where it con-

denses and releases its latent heat h_{fg} to the liquid. The liquid is in turbulent agitation. We restrict our attention to cases where the turbulence near the interface is the result of some mixing process or shear flow in the bulk of the liquid, deep below the surface, and not due to surface shear exerted by a horizontal vapor flow. Solid boundaries are remote from the free surface (i.e. many turbulence macroscales away) and do not affect the local condensation rate directly, although they may play a role in the energy balance that controls the 'bulk' liquid subcooling. Both the liquid-side turbulence and the condensation heat transfer process are assumed to have reached statistically steady states.

Below the free surface there will be an interfacial layer, about one turbulence macroscale thick, in which the turbulence and temperature distributions are strongly affected by the interfacial boundary conditions. As one approaches the interface from below, the vertical velocity fluctuations will tend to be damped and the horizontal fluctuations amplified, and the mean temperature will rise rapidly from the bulk to the saturation value. It is our premise that the local condensation rate can be completely specified in terms of the fluid properties and the turbulence conditions 'imposed' on the interface just below the interfacial layer. This is a high Reynolds number (and not too low Prandtl number) modeling approximation made in the spirit of dealing with interfacial layers in terms of inner and outer expansions. It leaves the question, however, of what constitutes a suitable definition of the 'imposed' turbulence. The turbulence in the bulk region, being generated from below, will necessarily decay in intensity with elevation even below the interfacial layer, but at a rate which is lower than in the interfacial region, as sketched in Fig. 7(a) (see also Section 3, and ref. [14]).

We make the following assumptions.

Turbulence. We assume that the turbulence 'at the surface' may be characterized by (1) the extrapolated value v_b of the turbulence intensity $v(y)$ from the bulk liquid region to the interface, ignoring the interfacial layer (Fig. 7(a)), (2) a similarly extrapolated turbulence macroscale Λ_b, (3) the liquid viscosity and (4) the liquid density. The first two define the large scales of the imposed turbulence; the last two, which are more specifically defined below, affect the energy cascade process and the small dissipative scales.

In our own experiments, the turbulence below the interfacial layer is approximately isotropic, and the quantity v_b is defined as the extrapolated r.m.s. value of any *single component* of the fluctuating velocity from the bulk to the surface.

Subcooling. The liquid subcooling is defined as

$$\Delta T \equiv T_s - T_b \tag{12}$$

where T_s is the saturation temperature and T_b the temperature obtained by extrapolating the mean temperature in the bulk of the liquid to the surface, ignoring the interfacial layer (Fig. 7(b)). The temperature gradient in the bulk liquid region is usually small compared with the gradient near the interface, and T_b can be interpreted as simply the local bulk temperature.

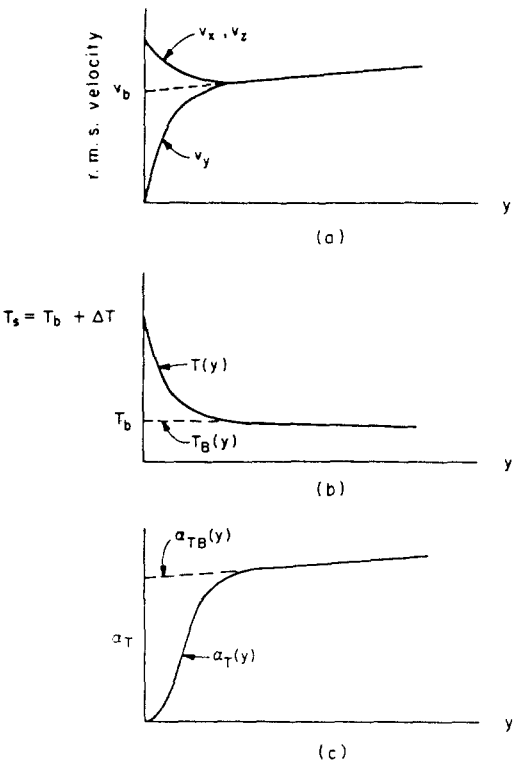

FIG. 7. Distributions of (a) r.m.s. velocity, (b) mean temperature, and (c) turbulent diffusivity. Definition of bulk values.

Liquid properties. The liquid properties which affect the condensation rate are the viscosity, density, thermal conductivity and specific heat. The density, specific heat and thermal conductivity of most liquids are relatively temperature insensitive, and we model these quantities as being uniform at their 'bulk' values ρ_b, c_{pb} and λ_b. (In water, for example, these three change by -7, 2 and 11%, respectively, as the temperature rises from 37 to 135°C, the maximum bulk to saturation temperature range in our experiments.)

Liquid viscosity is highly temperature dependent, however, and may vary significantly in the interfacial layer. In water, μ decreases by a factor of three as the temperature rises from 37 to 135°C. This temperature dependence should strictly speaking be accounted for in the scaling laws, since reduced viscosity in the hot interfacial layer may in principle affect the turbulence structure in that critical region, and hence influence the condensation rate. We do this by noting that the free volume theory of Hildebrand [19, 20] suggests that the viscosity of a liquid can be fitted over some range of temperatures and pressures with an equation of the form

$$\mu^{-1} = A + BT \tag{13}$$

where A and B are constants. For all liquids in which equation (13) applies between the bulk temperature T_b and the saturation temperature T_s, the viscosity can be expressed between those temperature limits as

$$(\mu_b/\mu) = 1 + (\mu_b/\mu_s - 1)(T - T_b)/\Delta T \tag{14}$$

where μ_b and μ_s are the viscosities at bulk and saturation conditions. Equation (14) is a good approximation for water between 37 and 135°C. For cryogenic liquids, the equation is usually a very good fit.

Equation (14) implies that the viscosity is completely specified by the temperature differential $T - T_b$ and the quantities μ_b, μ_s and ΔT.

Buoyancy and thermal stratification. Buoyancy effects will be accounted for in the Boussinesq approximation, where the buoyancy force in the equation of motion is expressed as $g\beta_b(T - T_b)$, g being either the acceleration of gravity or an applied acceleration normal to the interface, and β_b being the liquid's bulk coefficient of thermal expansion. We characterize β by its bulk value (an approximation), even though β depends significantly on temperature in many liquids and may have a different value in the hotter region near the interface. The bulk value is chosen because we are mainly interested in being able to properly scale the onset of buoyancy effects, and less concerned with accurately scaling conditions where a hot stagnant layer has developed on the surface.

Surface waviness. Surface waviness, always present to some degree on a turbulent liquid, is assumed not to affect the condensation mass flux. In our experiments, the amplitude v_b^2/g of the turbulence-induced waviness was small compared with the turbulence macroscale (wavelength) Λ_b, that is, $v_b^2/g\Lambda_b \ll 1$. Under these conditions, the surface is approximately horizontal, at least in the sense that its radius of curvature is large compared with the thermal layer thickness at the interface, and the condensation process will not depend on g except via the product $\beta_b g$ which characterizes the buoyancy effects.

Vapor properties. The condensation is assumed to be controlled by the rate at which the latent heat h_{fg} is transferred from the interface to the bulk of the liquid, and unaffected by any other vapor phase property. This is true if (i) the vapor's superheat and kinetic energy do not add significantly to the energy flux from the interface into the liquid, i.e. if $c_{pg}(T_g - T_s)/h_{fg} \ll 1$ and $\dot{m}^2/\rho_g^2 h_{fg} \ll 1$, and (ii) the momentum flux associated with the vapor's impact on the surface does not alter the liquid-side turbulence, i.e. if $\dot{m}^2/\rho_g\rho_b v_b^2 \ll 1$. Here, $\dot{m}$ is the condensation mass flux and the subscript g refers to vapor phase properties.

These criteria are satisfied in typical condensation problems unless the vapor is very highly superheated. Chun *et al.* [21] have shown that violations may also occur at very high turbulence intensity and/or subcooling, where the condensation can become unstable, and transient, very high-intensity condensation bursts can occur. Such condensation bursts are not covered by the scaling laws discussed here.

Based on the model presented above, the condensation mass flux will have the following dependence:

$$\dot{m} = f(v_b, \Lambda_b, \mu_b, \mu_s, \rho_b, \lambda_b, c_{pb}, \Delta T, h_{fg}, \beta_b g). \tag{15}$$

It follows immediately from dimensional analysis that

$$St = f(Re, Ri, Pr_b, Pr_s, Ja) \tag{16}$$

where

$St \equiv \dot{m}h_{fg}/\rho_b c_{pb}\Delta T v_b$ = condensation Stanton number

$Re \equiv \rho_b v_b \Lambda_b/\mu_b$ = turbulent eddy Reynolds number

$Ri \equiv \beta_b g \Delta T \Lambda_b / v_b^2$ = Richardson number based on turbulence intensity

$Pr_b \equiv \mu_b c_{pb}/\lambda_b$ = bulk Prandtl number

$Pr_s \equiv \mu_s c_{pb}/\lambda_b$ = saturation Prandtl number

$Ja \equiv c_{pb}\Delta T/h_{fg}$ = Jakob number. (17)

Strictly speaking there should be in equation (17) a sixth parameter which can be taken as $v_b^2/c_{pb}\Delta T$. It can be shown that this parameter is essentially the ratio of the heat input which results from turbulent viscous dissipation to the heat input which results from the latent heat. Heating due to turbulent viscous dissipation is negligible in most condensation problems, and hence this parameter should not affect the Stanton number.

The eddy Reynolds number will be large in all cases where the liquid side is fully turbulent. The Richardson number scales the buoyancy effects. In a gravitational field buoyancy effects tend to dampen the turbulence near a condensation interface, and to reduce the condensation rate. Based on data for analogous mixing processes [22, 23], one expects that the effect will be negligible if the Richardson number is smaller than some critical value of order unity, and significant at higher Richardson numbers. The bulk Prandtl number Pr_b scales the thermal and viscous diffusivities. The saturation Prandtl number Pr_s must be included if the viscosity difference between saturation and bulk conditions has a significant effect on the smaller scale turbulence structure near the interface. The effect of the Jakob number is discussed in Section 6 below.

Equations (16) and (17) reduce essentially to the scaling laws of Sonin *et al.* [9] if buoyancy effects are negligible. The present derivation is, however, more rigorous and explicit in its assumptions.

6. AN ANALYSIS

One impediment to a purely empirical determination of the functional form of equation (16) is the fact that both the Richardson and the Jakob numbers depend on ΔT. We shall attempt to separate these

dependencies by means of the following analysis for the Jakob number dependence, which is an elaboration of the one used by Sonin *et al.* [9].

The Jakob number scales the feedback effect of the condensation-induced bulk flow on the condensation rate. This can be seen by noting that the thermal layer thickness δ, i.e. the effective thickness of the region in which the temperature drops from T_s to T_b, is by definition

$$\dot{m}h_{fg} \equiv \lambda_b \Delta T/\delta. \tag{18}$$

Using equations (17) and (18), we can write the Jakob number as

$$Ja = u_c \delta/\alpha_b \tag{19}$$

where

$$u_c = \dot{m}/\rho_b \tag{20}$$

is the bulk flow speed induced on the liquid side by the condensation. The Jakob number is thus essentially the Peclet number based on the condensation-induced flow speed and the thermal layer thickness. This suggests that the condensation rate should decrease as the Jakob number increases, the flow velocity being in the direction of the heat flux.

A more quantitative idea of the Jakob number effect can be obtained by the following relatively simple theory. In the absence of mean liquid flow parallel to the surface (as in our experiments), the Reynolds-averaged temperature $T(y)$ in the liquid is given by

$$u_c \frac{\partial T}{\partial y} = \frac{\partial}{\partial y}\left[(\alpha + \alpha_T)\frac{\partial T}{\partial y}\right] \tag{21}$$

where y is the distance measured from the interface toward the bulk of the liquid, u_c the condensation-induced flow speed given by equation (20), and

$$\alpha_T \equiv -\frac{\langle v'T'\rangle}{\dfrac{\partial T}{\partial y}} \tag{22}$$

is the turbulent thermal diffusivity, $\langle v'T'\rangle$ being the Reynolds-averaged turbulent heat flux divided by ρc_p.

Equation (21) is subject to the boundary conditions

$$T(0) = T_s$$

$$\rho_b u_c h_{fg} = -\rho_b c_{pb}\alpha_b(\partial T/\partial y)_{y=0}. \tag{23}$$

An integration of equation (21) yields

$$\ln\left[1 + \frac{c_{pb}(T_s - T)}{h_{fg}}\right] = u_c \int_0^y \frac{dy}{\alpha + \alpha_T}. \tag{24}$$

The distribution of the 'bulk' liquid temperature $T_B(y)$ satisfies equation (21) with α_T equal to the thermal diffusivity α_{TB} in the bulk (see Fig. 7(c)). Integrating this equation from $y = 0$, where $T_B \equiv T_b$ (Fig. 7(b)), we obtain

$$\ln\left[\frac{1 + \dfrac{c_{pb}(T_s - T_B)}{h_{fg}}}{1 + Ja}\right] = u_c \int_0^y \frac{dy}{\alpha + \alpha_{TB}}. \tag{25}$$

The difference between equations (24) and (25) yields

$$\ln\left[\frac{\left(1 + \dfrac{c_{pb}(T_s - T)}{h_{fg}}\right)}{\left(1 + \dfrac{c_{pb}(T_s - T_B)}{h_{fg}}\right)}(1 + Ja)\right] = u_c \int_0^y \frac{(\alpha_{TB} - \alpha_T)}{(\alpha + \alpha_T)(\alpha + \alpha_{TB})}\,dy. \tag{26}$$

Now, for y larger than the interfacial layer thickness, $T(y) \Rightarrow T_B(y)$ and $\alpha_T(y) \Rightarrow \alpha_{TB}(y)$, and equation (26) reduces to an equation for u_c, which can be converted to an equation for St via equations (20) and (17). The result is

$$St = St_0 \frac{\ln(1 + Ja)}{Ja} \tag{27}$$

where

$$St_0^{-1} \equiv v_b \int_0^\infty \frac{(\alpha_{TB} - \alpha_T)\,dy}{(\alpha + \alpha_T)(\alpha + \alpha_{TB})}. \tag{28}$$

If it were now possible to argue that the condensation-induced flow speed u_c does not affect the turbulent diffusivity $\alpha_T(y)$ significantly, at least at small Jakob numbers, one could conclude that the function St_0 should be independent of Jakob number, i.e.

$$St_0 = f(Pr_b, Pr_s, Ri, Re). \tag{29}$$

Equations (27) and (29) would then give the Jakob number dependence of St. For $Ja \ll 1$, one has

$$St \simeq St_0(1 - Ja/2) \tag{30}$$

which shows that St_0 represents the Stanton number in the limit $Ja \Rightarrow 0$, and that the Jakob number effect is small as long as $Ja \ll 1$.

Equations (29) and (30) are based on the assumption that the turbulent diffusivity is not significantly affected by the condensation drift speed u_c if $Ja \ll 1$. More specifically, the assumption is that the first-order correction term due to the dependence of St_0 on Ja be small compared with $Ja/2$. Whether this is in fact so cannot be proved conclusively until we have a better understanding of the turbulence near the free surface. In the present study the Jakob number was small (of the order of 0.1) and its effect on the condensation was also small. However, it turns out that our data correlates somewhat better with the assumption that St_0 is independent of Jakob number than with the assumption that the Jakob number effect on St is negligible. We therefore adopt equations (29) and (30) as a working hypothesis.

Some further insight into the condensation process

may be obtained by noting that when equation (22) is expanded in Taylor series about $y = 0$, and the boundary conditions at the free surface applied (zero shear, zero vertical velocity, uniform temperature at the surface), one finds that the first non-zero term is of the order of y^2

$$\alpha_T = \frac{y^2}{\tau} + O(y^3) \quad (y \Rightarrow 0) \tag{31}$$

where τ is a statistical property, with dimension time, of the turbulent velocity and temperature fluctuations at the interface

$$\tau^{-1} \equiv \left\langle \frac{\partial T'}{\partial y} \frac{\partial v'}{\partial y} \right\rangle_{y=0} \left(- \frac{\partial T}{\partial y} \right)^{-1}. \tag{32}$$

If we take as a working approximation for $\alpha_T(y)$ for all y the equation

$$\frac{1}{\alpha_T(y)} = \frac{\tau}{y^2} + \frac{1}{\alpha_{TB}(y)} \tag{33}$$

which gives the correct results for both the limits of small and large y, and if we assume that $\alpha_{TB} \gg \alpha$ everywhere, equation (28) simplifies to

$$St_0^{-1} \simeq v_b \int_0^\infty \frac{dy}{\alpha + \frac{y^2}{\tau}} \tag{34}$$

or

$$St_0 = \frac{2}{\pi v_b} \left(\frac{\alpha}{\tau} \right)^{1/2}. \tag{35}$$

This does not solve the problem, but simply reduces it to that of determining the time scale τ as a function of turbulence characteristics and fluid properties. Results similar to equation (35) have been derived by King [3], Ledwell [24], and others. Our derivation emphasizes the point that, provided the molecular diffusivity α is everywhere small compared with the turbulent diffusivity α_{TB} associated with the bulk liquid, the quantity St_0 is unaffected by $\alpha_{TB}(y)$, regardless of the thickness of the interfacial thermal layer. Equations (31) and (35) link the condensation rate to the turbulent diffusivity distribution near the interface.

7. CONDENSATION RATE CORRELATION

The experimental variables over which we exercised control were four: bulk temperature T_b (via the heat exchanger), saturation temperature T_s (via system pressure), liquid-side turbulence intensity v_b, and turbulence macroscale Λ_b. v_b is taken as the *average* value over the free surface (see equations (3) and (6))

$$v_b \equiv (v_b)_{av} = 21.1(Q/Dd)\, e^{-1.2 z_s/D}. \tag{36}$$

The macroscale is given in terms of system diameter by equation (10).

Table 2. Test matrix for condensation tests (see Figs. 9–11)

(a) Symbols for test conditions

T_b (°C)	T_s (°C) 135	103
37	●	○
57	■	□
71	▲	△
82	▼	▽
118	★	

With line through data points: $D = 3.8$ cm.
Without line through data points: $D = 10.2$ cm.

(b) Prandtl number

Pr_b	Pr_s 1.3	1.7
4.65	●	○
3.15	■	□
2.55	▲	△
2.2	▼	▽
1.5	★	

With line through data points: $D = 3.8$ cm.
Without line through data points: $D = 10.2$ cm.

(c) Jakob number

Pr_b	Pr_s 1.3	1.7
4.65	0.19	0.12
3.15	0.15	0.09
2.55	0.13	0.06
2.2	0.11	0.04
1.5	0.03–0.06	

Table 2 summarizes the bulk and saturation temperatures chosen for the test matrix and lists the corresponding liquid Prandtl and Jakob numbers.

Figure 8 shows typical data of condensation mass

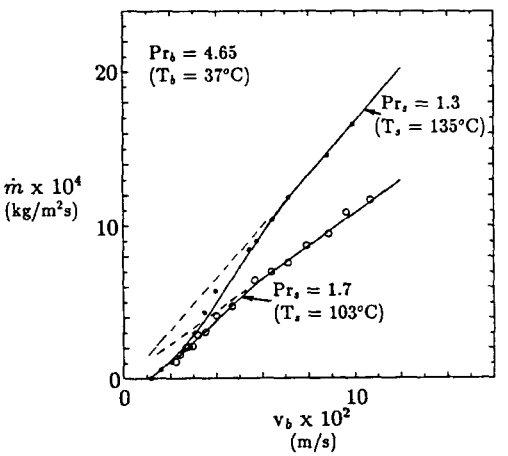

FIG. 8. Condensation mass flow rate vs turbulence intensity for steam and water at $Pr_b = 4.65$ ($T_b = 37$°C).

flux vs liquid-side turbulence intensity v_b, taken in the larger system ($D = 10.2$ cm) at constant bulk and saturation conditions. The upper bound of v_b is controlled by the requirement that the amplitude of the surface waves remain small (below about 1/2 cm in the larger system, as determined by visual inspection), so that the interfacial area can be approximated as $\pi D^2/4$. Note that the two data sets have different saturation conditions and therefore different subcooling.

In what follows we present all data in terms of the modified Stanton number

$$St_0 = St\left(1+\frac{Ja}{2}\right) \tag{37}$$

which is assumed to be independent of Jakob number. Some support for this independence may be deduced from the data correlation (see the discussion at the end of this section).

The Reynolds and Richardson number dependencies are at first sight difficult to separate because both these numbers vary with the experimental variables. It appears, however, that the condensation Stanton number is insensitive to Reynolds number. Figures 9 and 10 show all our data for St_0, plotted first against Reynolds number and then against Richardson number. Re and Ri are related by

$$Ri = Gr \cdot Re^{-2} \tag{38}$$

where the Grashof number

$$Gr \equiv \beta_b \Delta T g \Lambda_b^3/\nu_b^2 \tag{39}$$

depends mainly on the system diameter via Λ_b.

All the data plots show the same trend. For given system size, the Stanton number reaches a constant (maximum) value at sufficiently high Re or sufficiently low Ri, but declines sharply when Re is reduced below a critical value, or when Ri becomes significant compared with unity. The decline may in principle be due to high Richardson number (i.e. damping of the turbulence by thermal stratification near the surface), low Reynolds number (i.e. damping of the turbulence by viscous effects), or both. A comparison of the data taken in the large and small systems suggests that viscous damping can be ruled out: both systems exhibit the same maximum values, and no decline from the maximum value occurs in the small system at Reynolds numbers where a decline was observed in the large system. On the Richardson number plots, the data from both systems collapse onto the same curve. The figures clearly imply that, at least in the range of Reynolds numbers investigated, the Stanton number depends on Richardson number and bulk Prandtl number but not on Reynolds number. In addition, the plots against Ri show no difference between the two values of saturation Prandtl number. Our data thus suggest that

$$St_0 \simeq St_0(Ri, Pr_b) \tag{40}$$

$$350 < Re < 11\,000$$

$$1.3 < Pr_s < 1.7$$

$$1.5 < Pr_b < 5$$

$$0.03 < Ja < 0.2.$$

The functional form of equation (40) is defined in Fig. 10, and summarized in Fig. 11.

The effect of thermal stratification was visible to the naked eye, particularly at low bulk temperatures and with back lighting which tended to give rise to a shadowgraph effect. At turbulence intensities where Ri was of the order of 1–3, say, one could observe a hot layer at the surface, a few millimeters thick, which was formed and then periodically swept away by an energetic eddy. At still lower v_b ($Ri \sim 10$), the turbulence was not intense enough to overcome the damping effects of the thermal stratification, and the hot layer would no longer be swept away. At the lowest turbulence intensities ($Ri \sim 50$), stagnant hot layers of the order of 3 cm thick were observed beneath the interface.

The limit $Ri \Rightarrow 0$ where the effect of thermal stratification is negligible may be obtained by extrapolating the data to $Ri = 0$. The result is shown in Fig. 12, and can be represented by the equation

$$St_0 = 0.0198 Pr_b^{-0.33} \quad (Ri \Rightarrow 0). \tag{41}$$

The bars in Fig. 12 represent our assessment of the uncertainty in determining the limit $Ri \Rightarrow 0$ from the data in Fig. 10.

At $Ri > 3.5$, on the other hand, the data for all Pr_b tend to fall approximately on a common curve (Fig. 11), which can be represented as

$$St_0 \simeq 0.0136 - 8.1 \times 10^{-4} Ri \quad (3.5 < Ri < 15). \tag{42}$$

Finally, some comments about our assumption that the modified Stanton number defined in equation (37) is independent of Jakob number, which would suggest that the Stanton number should depend on Ja according to

$$St \simeq St_0(1 - Ja/2) \quad (Ja \ll 1). \tag{43}$$

Figure 13 shows three data sets of St vs Ja. Each set is taken at constant Pr_b and essentially constant Re. The Jakob number was varied by changing the saturation temperature from 140 to 102°C (Pr_s from 1.25 to 1.7). Within each set the Richardson number varies with the Jakob number, but remains relatively small throughout the data range (see Table 3), so that its effect on St_0 is not large. Also shown on the figure are 'theoretical' curves based on equation (43) with St_0 taken from Fig. 10. The agreement between experiment and 'theory' is satisfactory. However, the dependence on Ja is so slight in our data that it is almost masked by the data scatter. We can say only that equation (43) appears to fit the data somewhat better than an assumption that St is independent of Ja.

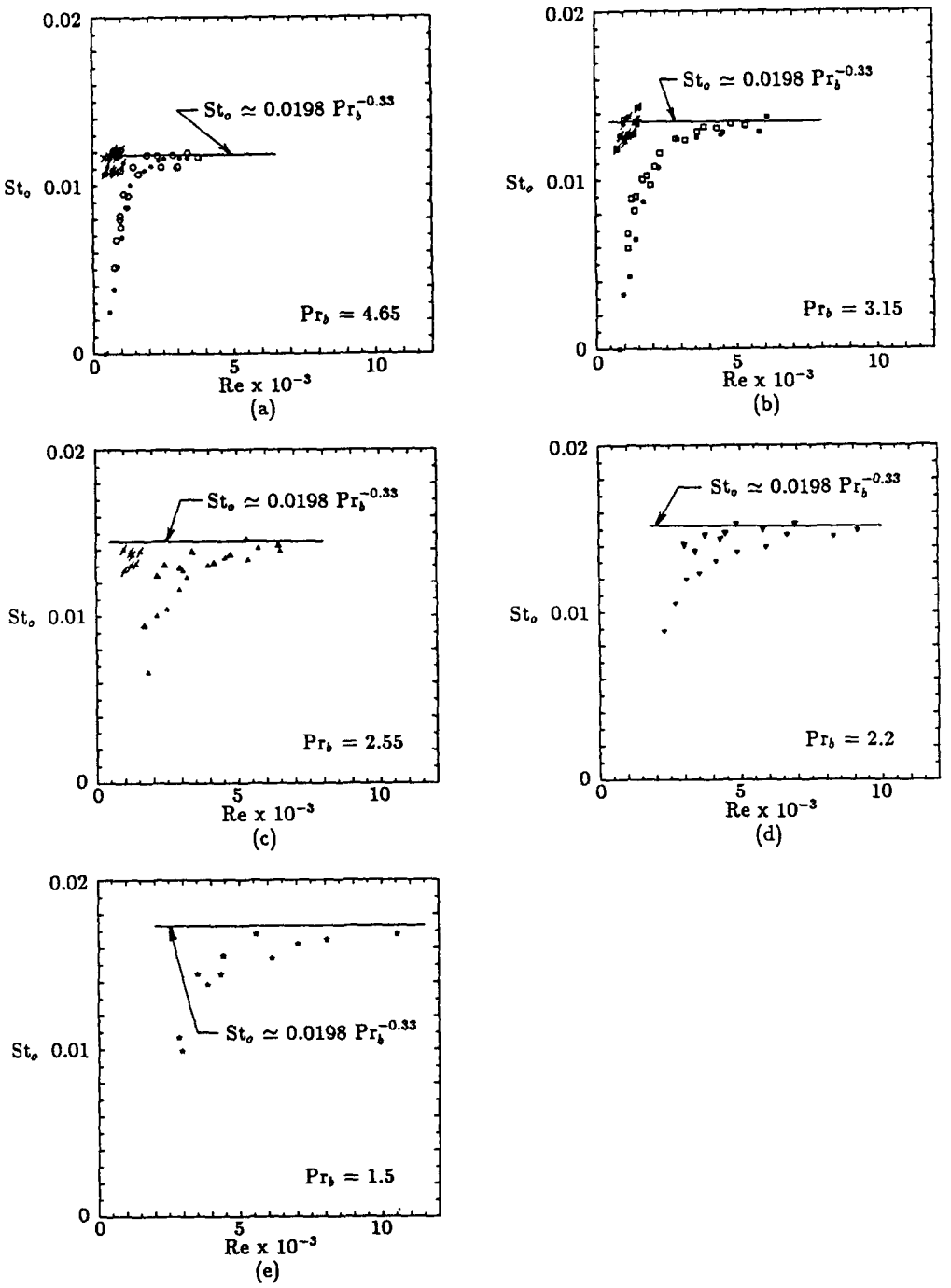

FIG. 9. Reduced Stanton number vs Reynolds number. See Table 2 for symbols.

8. CONCLUDING REMARKS

Our data suggest a condensation rate correlation of the form

$$St = St_0(Ri, Pr_b)(1 - Ja/2) \tag{44}$$

where the modified Stanton number St_0 is given in Fig. 10. The data correlation should be applicable for

$$\begin{aligned} 350 < Re < 11\,000 \\ Ri < 15 \\ 1 < Pr_b < 6 \\ 1 < Pr_s < 2 \\ Ja < 0.2. \end{aligned} \tag{45}$$

These conditions apply not only to steam and water but also to most cryogenic fluids at normal pressures.

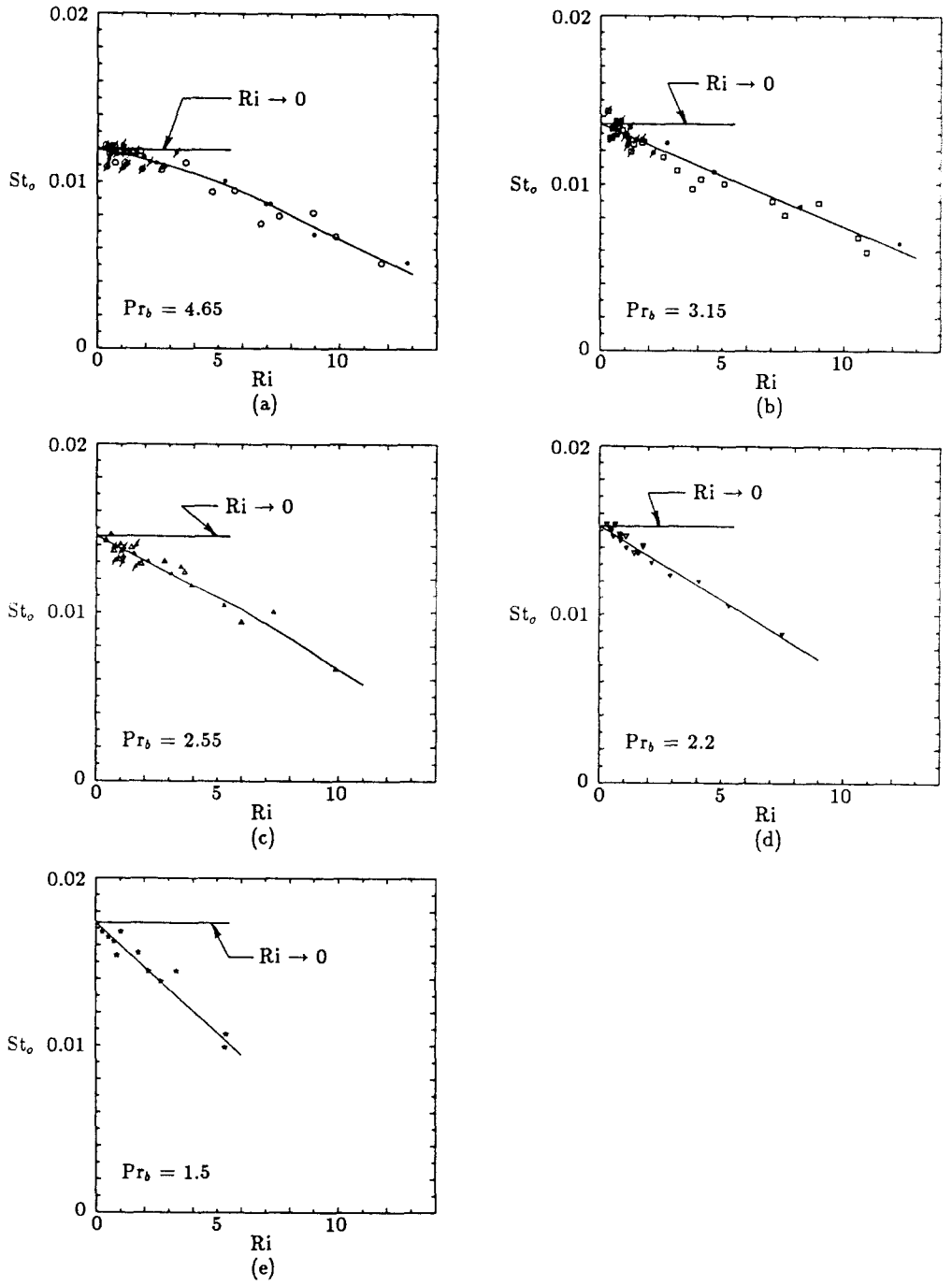

FIG. 10. Reduced Stanton number vs Richardson number. See Table 2 for symbols.

In the limit $Ri \Rightarrow 0$ of negligible buoyancy effects, St_0 is given by equation (41), and the condensation heat transfer process can be represented in terms of a Reynolds-averaged energy equation with a turbulent diffusivity given near the interface by

$$\alpha_T/\nu = 9.67 \times 10^{-4}(v_b y/\nu)^2 Pr_b^{0.34}. \quad (46)$$

Equation (46) follows from equations (31), (35) and (41). The Stanton number begins to fall below equation (41) when Ri reaches values of the order of 1.2. This is consistent with studies of turbulence structure in stably stratified flows [13, 15, 16, 22, 23]. At $Ri > 3.5$, St_0 appears to become relatively insensitive to the bulk liquid Prandtl number and is given approximately by equation (42).

The Prandtl number dependence in equation (41) differs from the correlation proposed by Sonin *et al.* [9], which had no dependence on Pr_b. Most of the

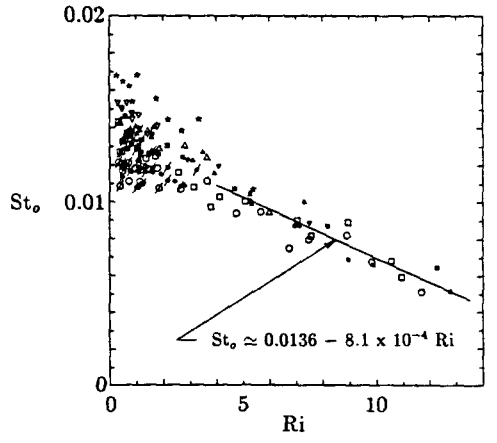

FIG. 11. Reduced Stanton number vs Richardson number. See Table 2 for symbols.

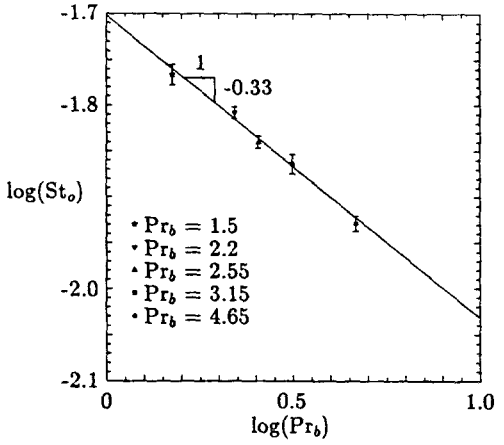

FIG. 12. Reduced Stanton number, extrapolated to $Ri \Rightarrow 0$, vs bulk Prandtl number.

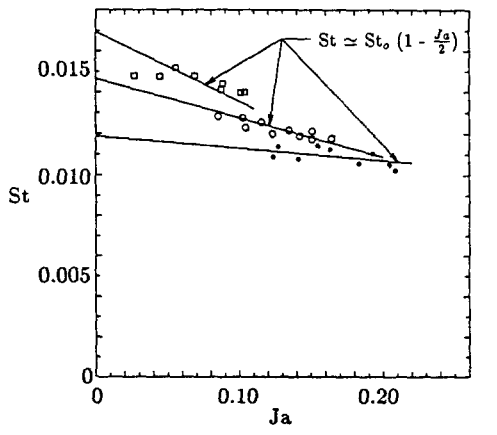

FIG. 13. Condensation Stanton number as a function of Jakob number. Data obtained by varying saturation temperature. See Table 3 for test conditions.

Table 3. Test conditions for Fig. 13

Symbol	T_b (°C)	Re	Ri
□	88	4370 ± 135	0.6–2.3
○	57	3020 ± 70	1.5–2.8
●	37	2300 ± 80	1.2–2.1

data on which their correlation was based were taken at relatively low bulk temperatures, where Pr_b had values of approximately 4–6. At $Pr_b = 5$, our equation (41) gives $St_0 \simeq 0.0116$, in good agreement with Sonin *et al.* [9] if one compensates for the fact that their correlation was based on the centerline r.m.s. velocity while our present one is based on the average value, which is 10% lower. Their conclusion about the lack of Pr_b dependence, however, was based on a small additional subset of data (their Fig. 11) which was taken at high bulk temperatures. We speculate that the apparent insensitivity to bulk temperature was in fact caused by the systematic thermistor error which we found present at high temperatures in the thermal method which Sonin *et al.* [9] used for measuring the condensation flux (see our Section 4).

To our knowledge the dependence on Prandtl number has not been previously measured for condensation at a turbulent free surface. Our present data indicates that at Prandtl numbers in the range 1.5–5, the index n in $St \sim Pr_b^{-n}$ is about 1/3. We note that the analogous exponent for the Schmidt number dependence in gas absorption at a liquid free surface is usually taken as $n \simeq 1/2$ (see for example Ledwell [24] and also Khoo [25], who performed mass transfer experiments in the same type of test cell as we used in our present work), although exponents as high as unity have been suggested [26]. Gas absorption is, however, a high Schmidt number transport problem, with $Sc \sim 500$. At a solid boundary, the Stanton number based on the friction velocity u_* is proportional to $Pr_b^{-2/3}$ at high Prandtl numbers [27].

Insofar as a quantitative comparison is possible [28], the present correlation is essentially in agreement with the steam condensation data of Thomas [10], where the turbulence was generated from below the interface. Our correlation is strictly speaking not intended for flows like Jensen and Yuen's [11], where the liquid-side turbulence is generated by shear at the free surface itself. Such turbulence is anisotropic and varies strongly near the surface, and cannot necessarily be adequately characterized by the quantities ν_b, Λ_b, and μ_b. Nevertheless, if a direct comparison is attempted [9], one obtains agreement within a factor of two.

None of the simple models which have been proposed for gas absorption can be adapted to explain both the velocity and Prandtl number dependence of our equation (41). This has led us to attempt a direct numerical simulation of the problem, based on the full unsteady Navier–Stokes equation and energy equation. The computational domain is one macro-

scale deep, and an artificially generated 'isotropic turbulence' is applied at the lower boundary, which is supposed to represent the 'bulk' liquid side [29]. While this simulation suffers from some problems which arise from the artificial lower boundary condition, the agreement with the present data is promising.

The Stanton number correlation presented in this paper expresses the free surface condensation rate in terms of fluid properties and two local attributes of the liquid-side turbulence below the interfacial layer, the r.m.s. velocity v_b and a macroscale Λ_b. These two parameters must be available if the correlation is to be applied in a particular case. In principle, v_b and Λ_b can be obtained (only v_b is required if Ri is small) from empirical scaling relations, where available, or from a computation of the liquid-side flow field based on a turbulence model. If Λ_b is required, it becomes necessary to first establish how this quantity is related to whatever macroscale appears in the particular empirical correlation or turbulence model that is being used. We expect that Λ will be proportional to any other definition of a macroscale, say l. The coefficient of proportionality can be obtained from a single calibration. If l is obtained from an experimental correlation, one must have available one simultaneous measurement of both l and Λ, or predict the relationship theoretically. If l is derived from a turbulence model, it will often lack a physical definition. In that case a numerical calibration is necessary for the ratio of Λ and l. The calibration can be achieved by exercising the chosen turbulence model on our test cell, and comparing the predicted l with our experimental calibration for Λ, equation (10). For example, Sonin *et al.* [9] made an attempt to determine the k–ε model length scale $L \equiv k^{3/2}/\varepsilon$ in the system of Fig. 1 by fitting a one-dimensional analytic solution of the k–ε model to their data for the axial distribution of v. They obtained the result that $L \simeq 1.1D$ for $3 < z/D < 4$, which suggested that $\Lambda_b \simeq 0.22L$. Their calibration can, however, be criticized on the grounds that a one-dimensional model neglects radial diffusion of turbulent kinetic energy to the walls. Recently, Hasan and Lin [30] solved the k–ε model for the complete axisymmetric system of Fig. 1, including the entire flow field from the nozzle exit upward. Their results indicate that with the surface at $z_s/D = 3.67$, L ranges from about $0.4D$ to $0.6D$ at the centerline, depending on depth below the interface, and drops to lower values near the walls. However, Hasan and Lin's calculations are not without problems of their own, and show what appear to be unrealistic predictions for large z/D. These apparently stem from the difficulty one encounters in applying proper boundary conditions for k and ε at the free surface. If our correlation is to be applied to cases where the Richardson number is not small, a means of predicting Λ is required. Further work is clearly needed in order to establish the ratio between Λ and the length scales that appear in the turbulence models which are applicable to free surface problems.

Acknowledgement—This work was supported by Grant NAG3-731 from NASA Lewis Research Center, and monitored by J. C. Aydelott, D. M. DeFelice and M. M. Hasan. One of us (B.C.K.) was supported by the Singapore government.

REFERENCES

1. M. Kh. Kishinevsky, Two approaches to the theoretical analysis of absorption processes, *J. Appl. Chem. USSR* **28**, 881–886 (1955) (translation pagination).
2. V. G. Levich, *Physicochemical Hydrodynamics*. Prentice-Hall, Englewood Cliffs, New Jersey (1962).
3. C. J. King, Turbulent liquid phase mass transfer at a free gas–liquid interface, *Ind. Engng Chem. Fundam.* **5**, 1–8 (1966).
4. G. E. Fortescue and J. R. A. Pearson, On gas absorption into a turbulent liquid, *Chem. Engng Sci.* **22**, 1163–1176 (1967).
5. J. C. Lamont and D. S. Scott, An eddy cell model of mass transfer into the surface of a turbulent liquid, *A.I.Ch.E. Jl* **16**, 513–519 (1970).
6. T. G. Theofanous, R. N. Houze and L. K. Brumfield, Turbulent mass transfer at free, gas–liquid interfaces, with application to open-channel, bubble and jet flows, *Int. J. Heat Mass Transfer* **19**, 613–624 (1976).
7. W. H. Henstock and T. J. Hanratty, Gas absorption by a liquid layer flowing on the wall of a pipe, *A.I.Ch.E. Jl* **25**, 122–131 (1979).
8. T. G. Theofanous, Conceptual models of gas exchange. In *Gas Transfer at Water Surfaces* (Edited by W. Brutsaert and G. H. Jirka), pp. 271–281. Reidel, Dordrecht (1984).
9. A. A. Sonin, M. A. Shimko and J.-H. Chun, Vapor condensation onto a turbulent liquid—I. The steady condensation rate as a function of liquid-side turbulence, *Int. J. Heat Mass Transfer* **29**, 1319–1332 (1986).
10. R. M. Thomas, Condensation of steam on water in turbulent motion, *Int. J. Multiphase Flow* **5**, 1–15 (1979).
11. R. J. Jensen and M. C. Yuen, Interphase transport in horizontal stratified concurrent flow, U.S. Nuclear Regulatory Commission Report NUREG CR-2334 (1982). Also in *Proc. 7th Int. Heat Transfer Conf.*, Vol. 5, pp. 95–100 (1982).
12. H. Ueda, R. Moller, S. Komori and T. Mizushina, Eddy diffusivity near the free surface of open channel flow, *Int. J. Heat Mass Transfer* **20**, 1127–1136 (1977).
13. T. Mizushina, F. Ogino, H. Ueda and S. Komori, Buoyancy effect on eddy diffusivities in thermally stratified flow in an open channel, *Proc. 6th Int. Heat Transfer Conf.*, Vol. 1, pp. 91–96 (1978).
14. S. Komori, H. Ueda, F. Ogino and T. Mizushina, Turbulence structure and transport mechanism at the free surface in an open channel flow, *Int. J. Heat Mass Transfer* **25**, 513–521 (1982).
15. S. Komori, H. Ueda, F. Ogino and T. Mizushina, Turbulence structure in stably stratified open-channel flow, *J. Fluid Mech.* **130**, 13–26 (1983).
16. F. Ogino, Turbulent flow and heat transfer with buoyancy effect, *Proc. 8th Int. Heat Transfer Conf.*, Vol. 1, pp. 69–78 (1986).
17. D. Coles, The law of the wake in the turbulent boundary layer, *J. Fluid Mech.* **1**, 191–226 (1956).
18. H. Tennekes and J. L. Lumley, *A First Course in Turbulence*. MIT Press, Cambridge, Massachusetts (1972).
19. J. H. Hildebrand, Motion of molecules in liquids: viscosity and diffusivity, *Science* **174**, 490–493 (1971).
20. J. H. Hildebrand, *Viscosity and Diffusion: a Predictive Treatment*. Wiley, New York (1977).
21. J.-H. Chun, M. A. Shimko and A. A. Sonin, Vapor condensation onto a turbulent liquid—II. Condensation burst instability at high turbulence intensities, *Int. J. Heat Mass Transfer* **29**, 1333–1338 (1986).

22. E. J. Hopfinger and J. A. Toly, Spatially decaying turbulence and its relation to mixing across density interfaces, *J. Fluid Mech.* **78**, 155–175 (1976).
23. X. E. Hopfinger and E. J. Hopfinger, On mixing across an interface in stably stratified fluid, *J. Fluid Mech.* **166**, 227–244 (1986).
24. J. J. Ledwell, The variation of the gas transfer coefficient with molecular diffusivity. In *Gas Transfer at Water Surfaces* (Edited by W. Brutsaert and G. H. Jirka), pp. 293–302. Reidel, Dordrecht (1984).
25. B. C. Khoo, A numerical and experimental study of the scalar transport at a turbulent liquid free surface, Ph.D. Thesis, Massachusetts Institute of Technology, Cambridge, Massachusetts (1988).
26. J. T. Davies, A. A. Kilner and G. A. Ratcliff, The effect of diffusivities and surface films on rates of gas absorption, *Chem. Engng Sci.* **19**, 583–590 (1964).
27. B. S. Petukhov, Heat transfer and friction in turbulent pipe flow with variable physical properties. In *Advances in Heat Transfer* (Edited by J. P. Hartnett and T. F. Irvine, Jr.), Vol. 6, pp. 503–564. Academic Press, New York (1970).
28. J. S. Brown, M. R. Helmick and A. A. Sonin, Vapor condensation at a turbulent liquid surface in systems with possible space-based applications, AIAA Paper 89-2846 (1989).
29. B. C. Khoo, A. T. Patera and A. A. Sonin, Direct numerical simulation of pure vapor condensation at a turbulent liquid interface: an extracted-subdomain approach. In *Heat Transfer With Phase Change* (Edited by I. S. Habib and R. N. Dallman), ASME HTD-Vol. 114, Book No. H00517 (1989).
30. M. M. Hasan and C.-S. Lin, Axisymmetric confined turbulent jet directed towards the liquid surface from below, AIAA Paper 89-0172 (1989).

FORMULE POUR LA CONDENSATION DE LA VAPEUR PURE SUR UN LIQUIDE SOUS-REFROIDI TURBULENT

Résumé—On présente une formule empirique pour la condensation de vapeur pure sur un interface de liquide sous-refroidi turbulent. La formule exprime la dépendance de la condensation vis-à-vis des propriétés des fluides, de la turbulence du liquide (qui est imposée par dessous) et des effets du flottement sur la couche thermique interfaciale. La formule est tirée des expériences avec l'eau et sa vapeur, mais sous des conditions qui simulent les fluides cryogéniques typiques.

KORRELATION FÜR DIE KONDENSATION EINES REINEN DAMPFES AN EINER TURBULENT STRÖMENDEN, UNTERKÜHLTEN FLÜSSIGKEIT

Zusammenfassung—Es wird eine empirische Korrelation für die Kondensation eines reinen Dampfes an einer unterkühlten, turbulent strömenden Flüssigkeit ohne Schubspannung an der Phasengrenze vorgestellt. Die Korrelation gibt die Abhängigkeit der Kondensationsstromdichte von den Stoffeigenschaften der Flüssigkeit, der flüssigkeitsseitigen Turbulenz (die von unten aufgeprägt wird) und von den Auftriebseffekten in der thermischen Grenzschicht wieder. Die Korrelation wurde aufgrund von Versuchen mit Dampf und Wasser aufgestellt, jedoch unter Bedingungen, die auch für typische kryogene Fluide gelten.

СКОРОСТЬ КОНДЕНСАЦИИ ЧИСТОГО ПАРА НА ТУРБУЛЕНТНОЙ НЕДОГРЕТОЙ ЖИДКОСТИ

Аннотация—Приводится эмпирическое соотношение, описывающее конденсацию чистого пара на недогретой тубулентной жидкости с межфазной границей без сдвига. Соотношение учитывает зависимость скорости конденсации от свойств жидкости и газа, турбулентности жидкости (которая налагается снизу) и эффектов подъемных сил в межфазном тепловом слое. Соотношение выводится на основе экспериментов с водяным паром и водой в условиях, моделирующих типичные криогенные жидкости.